Efficiency Enhancement of Synthetic Jet Actuators using Single Crystal Piezoceramics

*Jabbal, M.**
University of Nottingham, NG7 2RD, UK
Dave, R.†
Wirth Research, Bicester OX26 4LD, UK
Nesvijski, E.‡
TRS Technologies, PA 16801, USA

Abstract

This report documents the first manufacture and test of a single crystal (PMN-PT) piezoceramic diaphragm synthetic jet actuator for more efficient operation. The experimental investigation included laser vibrometry for diaphragm displacement measurement and hotwire anemometry for jet velocity measurement, as well as measurements of electrical power input to the disc. The performance of the single crystal device was compared with a synthetic jet actuator using a polycrystalline (PZT-5A) disc of the same geometry. For a fixed diaphragm drive voltage (20 V), the diaphragm displacement of PMN-PT is five times larger than PZT-5A. For comparable jet velocities (~40 m/s), the power conversion efficiency of the PMN-PT device is two times larger than the PZT-5A device. Finally, for comparable power conversion efficiencies (~20%), the peak jet velocity of the PMN-PT device is two times larger than the PZT-5A device.

Nomenclature

Speed of sound – a [m/s]
Orifice Area – A [m^2]
Orifice Diameter – d [mm]
Cavity Diameter – D [mm]
Electric Power – E [W]
Young's Modulus – E [GPa]
Electric field strength – E_c [kV/cm]
Disc excitation frequency – f [Hz]
Airflow (fluidic) power – F [W]
Orifice height – h [mm]
Cavity Height – H [mm]
Current – I [A]
Electromechanical coupling coefficient – k [-]
Diaphragm clamping condition – k^2 [-]
Diaphragm radius – r [mm]
Instantaneous time – t [s]
Diaphragm thickness – t [mm]
Jet velocity – U [m/s]
Voltage – V [Volts]
Dielectric loss coefficient – tan δ [%]
Disc peak-to-peak displacement – Δ [μm]
Electric-to-fluidic power efficiency – η [%]
Phase angle – φ [rad]
Energy transmission coefficient – λ [-]
Poisson's ratio - ν [-]
Density – ρ [kg/m^3]
Diaphragm damping coefficient – ξ [-]

1 Introduction

SYNTHETIC jet actuators (SJAs) consist of a moving diaphragm, pressure chamber and orifice plate, as illustrated in Figure 1. When actuated, the diaphragm typically deforms in a sinusoidal manner to create pressure fluctuations in the cavity, hence creating a cycle of expulsion and suction strokes through the orifice. For this reason, the SJA is a zero-net-mass flux device, but a non-zero-momentum flux device. It is this characteristic that makes it potentially suitable as an active flow control (AFC) device for aircraft applications such as separation control for drag reduction.

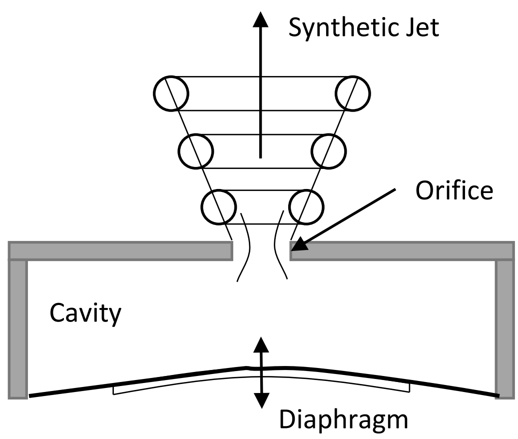

Figure 1. Synthetic jet actuator

There is a major challenge in getting sufficient power density from SJAs to deliver reasonable authority whilst meeting volume installation requirements of commercial aircraft. It is one of the reasons to-date why adoption of SJAs, and AFC more generally, for aircraft is still far off. Indeed, SJAs were overlooked for full-scale flight-testing on the B757 'ecoDemonstrator' aircraft for drag reduction on the vertical tail for reasons of low jet authority and low overall actuator efficiency [1].

It seems logical that the best overall improvements are likely to be made when the AFC system is incorporated in a systematic manner with other systems, in order to maximise the advantage obtained. Electrically powered AFC systems offer potential for greater synergistic benefits (i.e. reduced system mass and space requirements) on board civil transport aircraft where the systems are predominantly (and increasingly) electric and where a power

---
* Assistant Professor
† Aerodynamics Engineer
‡ Senior Scientist

distribution system already exists. The level of maturity of electrical systems is such that they form an appropriate AFC technology platform for aircraft with entry-into-service in the medium- to long-term – a realistic timeframe for the adoption of AFC devices. From an electrical input, there are several methods of displacing a volume of fluid through an orifice, as a means to creating a synthetic jet flow. These methods comprise of the following SJAs:

- Piezoceramic (PZT) [2]: electro-mechanical-fluidic transduction.
- Electro-active polymer (EAP) [3]: electro-mechanical-fluidic transduction.
- Ferromagnetic shape memory alloy (FSMA) [4]: electro-magneto-mechanical-fluidic transduction.
- Plasma synthetic jet actuator (PSJA) [5]: electro-magneto-hydrodynamic transduction.

Figure 2 compares actuator power densities of the different SJAs. Power specific mass and power specific volume are evaluated from the fluidic power delivered by the actuator against the mass and volume of the actuator unit. Fig. 2a shows that both PZT and FSMA SJAs have comparable power specific masses. However, PZT has a significantly higher power specific volume relative to the other actuators (Fig. 2b): PZT ~O (100), PSJA ~O (10), FSMA ~O (1) and EAP ~O (0.1). From Fig. 2, the leap in power density required to meet volume installation requirements is relatively small for PZT-based SJA, thereby making it the most viable SJA for implementation.

(a)

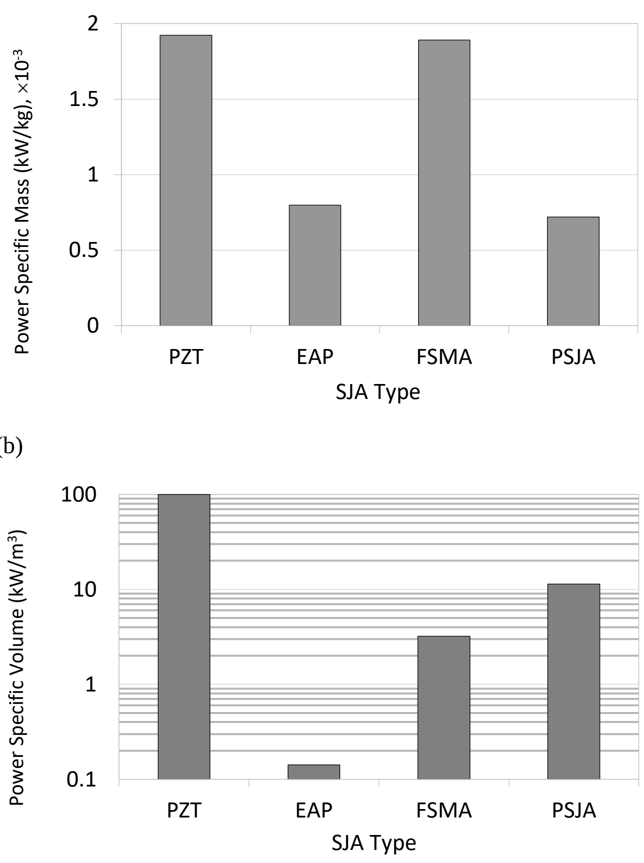

Figure 2. (a) Power specific mass and (b) power specific volume for various SJA types

One of the key issues of piezoceramic-based SJAs is the relatively low electric-to-fluidic power conversion efficiency. Table 1 shows such efficiencies of SJAs that have been reported in the literature. It can be seen that, generally, there is an inverse relation between the diaphragm drive voltage, V_{peak} (and therefore peak jet velocity, U_{peak}) and the electric-to-fluidic power conversion efficiency, η. Crowther and Gomes [2] showed that there was no co-location of conditions between peak jet velocity and peak efficiency, which is consistent with dielectric saturation of the piezoelectric patch. In all the reported cases highlighted in Table 1, the diaphragms used consist of a polycrystalline piezoceramic patch (PZT) bonded to a metal shim (mainly brass), due to their low cost and commercial availability. The diaphragms have a nominal peak drive voltage of V_{peak} = 15 V [6].

Table 1 Comparison of SJA peak jet velocities and efficiencies obtained from experiments (*2D slot dimensions)

Ref	d (mm)	D (mm)	V_{peak} (Volts)	U_{peak} (m/s)	η (%)
[2]	1.2	25	125 (45)	130 (70)	7 (14)
[7]	1×12*	80	150	120	3.5
[8]	2	30.8	100	50	45
[9]	1	25	50	38	15
[10]	1×4*	30	80	35	25
[11]	5	80	35	25	63

Buren et al. [7] have reported U_{peak}=211 m/s from their SJA, which is believed to be the highest SJA U_{peak} recorded to-date. However, this was achieved with a dual diaphragm configuration. In addition, no efficiency was reported for this case, but it is anticipated to be less than η=3.5% reported for U_{peak}=120 m/s, as shown in Table 1. It has been shown that the ratio of peak jet velocity to local free stream velocity (VR) required for effective rudder separation control is VR=3 [12]. While the SJA authority reported by Buren et al. [7] may be close to achieving VR=3 (based on a local free stream velocity of U_∞=70 m/s over the rudder), the low efficiency means that the overall system mass and power consumption associated with an array of SJAs is likely to be too prohibitive to do so.

Polycrystalline piezoceramic, such as lead zirconate titanate (PZT), has low electromechanical coupling, resulting in a majority energy that is either stored (the piezoceramic effectively acting as a capacitive energy-storing device) or lost in the electromechanical conversion. Figure 3 shows the breakdown of the main losses incurred in a SJA operating in quiescent conditions. Only 40 per cent of the electric power supplied to a PZT is converted to mechanical energy in the form of diaphragm vibrations.

Conversely single crystal piezoceramic, such as lead magnesium niobate-lead titanate (PMN-PT), exhibit much higher (typically 30%) electromechanical coupling resulting in more energy transfer to the diaphragm for a given input voltage. Rusovici and Lesieutre [13] conducted numerical modelling of a PMN-PT SJA and compared its velocity output with a PZT-5A SJA. It was found that for the same input voltage, the peak jet velocity of the PMN-PT SJA was greater than the PZT-5A SJA by about 40%. However, to-date there is no known experimental comparison between the performance of polycrystalline and single crystal SJAs. Compared with polycrystalline piezoceramic, single crystal piezoceramic is much more expensive and mechanically weaker due to the absence of grain boundaries, which makes manufacture of thin single crystal discs more complex.

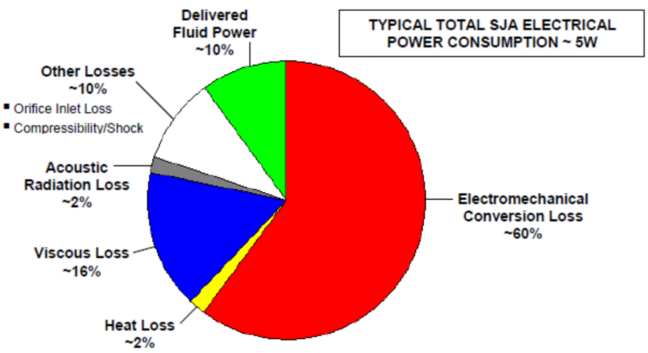

Figure 3. Breakdown of the main SJA losses [14]

The aim of this work is to compare, experimentally, the performance of a single crystal diaphragm SJA with a polycrystalline diaphragm SJA. Specifically, the objectives of this work include:

- Outsource the custom manufacture of a single crystal diaphragm (PMN-PT), to match the geometry of a commercial-off-the-shelf, polycrystalline diaphragm (PZT-5A).
- Integrate diaphragms into a common SJA geometry and conduct frequency sweep tests in quiescent conditions to compare (at the same input voltage): diaphragm displacement, peak jet velocity, and electric-to-fluidic power conversion efficiency.

2 Theory

2.1 Actuator Figures of Merit

The electromechanical coupling factor, k, is the effectiveness with which a piezoceramic converts electrical into mechanical energy and is given by Eq. (1)

$$k = \frac{stored\ mechanical\ energy}{input\ electrical\ energy} \tag{1}$$

Not all of the stored energy can be used, and the actual work done depends on the load. The energy transmission coefficient, λ, is accordingly defined by Eq. (2)

$$\lambda = \frac{output\ mechanical\ energy}{input\ electrical\ energy} \tag{2}$$

Finally, the SJA power conversion efficiency, η, is given by Eq. (3)

$$\eta = \frac{output\ fluidic\ power}{input\ electrical\ power} \tag{3}$$

2.2 Power Conversion Efficiency

The power supplied to a SJA can be considered as electrical energy input, E. Some of this energy is stored as electrical potential energy because of the electric capacitance of the piezoceramic diaphragm. The remaining energy is converted to mechanical energy along with energy loss. The mechanical energy of the actuator can be considered as the vibration of the piezoelectric diaphragm plus the synthetic jet exiting the orifice. It is necessary to determine the electric-to-fluidic power conversion efficiency of the SJA and so the mechanical energy of the diaphragm due to vibration is not considered. It is assumed that the static pressure and specific volume of air at the orifice are the same as the ambient. Therefore, the energy of airflow exiting the orifice is equal to its kinetic energy, F. The energy loss of the SJA is incurred due to the deflection of the diaphragm as well as some energy loss in the airflow prior to exiting the orifice, as illustrated in Fig. 3. The efficiency of energy conversion for synthetic jets, η, is the ratio of the output and input energy given by Eq. (4)

$$\eta = \frac{\dot{F}}{\dot{E}} \tag{4}$$

To calculate efficiency it is necessary to determine the flow power. The airflow power for a SJA [10] is given by Eq. (5)

$$\dot{F} = \frac{1}{2}\rho A U^3 \tag{5}$$

Where A is the orifice area, ρ is the density of air and U is the synthetic jet velocity. The power input applied to the piezoelectric diaphragm depends on the voltage amplitude. Due to the electrical capacitance of the diaphragm, there is a phase angle difference between the voltage and current. Because of that, the current signal has a time delay that varies over a range of frequencies. The phase angle, φ, is given by Eq. (6)

$$\varphi = 2\pi f \Delta t \tag{6}$$

The instantaneous true power input is calculated in Eq. (7) as

$$\dot{E} = V_{peak} I_{peak} \sin(2\pi f t) \sin(2\pi f t + \varphi) \quad (7)$$

Where V_{peak} and I_{peak} is the peak voltage and peak current respectively, f is the excitation frequency and t is the instantaneous time.

Since it is common to express velocities in terms of peak jet velocity, U_{peak}, then the flow and electrical power should be calculated at peak values (F_{peak} and E_{peak} respectively). It is thus necessary to obtain an expression for the peak electrical power. From trigonometry

$$V_{peak} I_{peak} \sin(2\pi f t) \sin(2\pi f t + \varphi) = \frac{1}{2} V_{peak} I_{peak} (\cos(\varphi) - \cos(4\pi f t + \varphi)) \quad (8)$$

Eq. (8) is a function of time and will give the maximum peak true power when $\cos(4\pi ft + \varphi) = -1$. The rest of the terms remain constant at a given frequency. Therefore, the peak power input, E_{peak}, can be expressed by Eq. (9)

$$E_{peak} = \frac{1}{2} V_{peak} I_{peak} (\cos\phi + 1) \quad (9)$$

Where $\cos\phi$ is the power factor, which is equivalent to the phase angle (Eq. (6)).

3 Experimental Approach

3.1 Piezoelectric Material and Manufacturing

Conventional piezoelectric materials used for mechanical energy generation are based on lead zirconate titanate (PZT) ceramics. Single crystal systems based on $PbMg_{1/3}Nb_{2/3}O_3 – PbTiO_3$ (PMN-PT) offer higher electromechanical coupling and approximately five to six fold increase in piezoelectric constant over PZT ceramics. The increase of over 30% in electromechanical coupling provides a significant improvement over current piezoceramic actuators for power conversion efficiency. These materials take advantage of anisotropy and crystallographic orientation dependent properties offered by single crystals. Current crystal growth for PMN-PT is in the [001] direction. Figure 4 shows the general schematic of crystal growing and Figure 5 shows the piezoelectric loop of the single crystal material, poled through the thickness [001].

3.2 Actuator Setup

The geometry of the piezoelectric diaphragm for both PZT-5A and PMN-PT is shown in Figure 6. As with the polycrystalline device, the single crystal piezoceramic was bonded to the brass shim using epoxy.

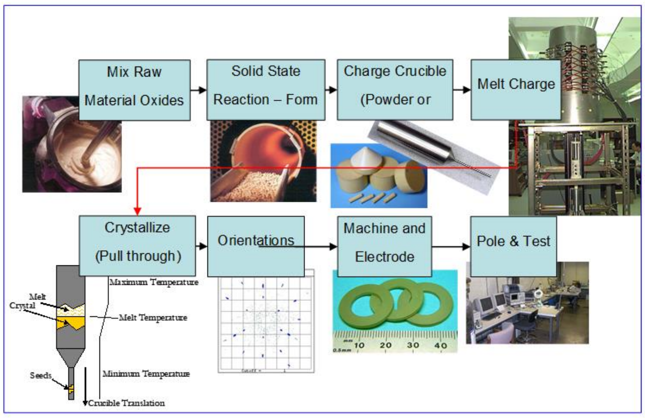

Figure 4. Single crystal growth and fabrication process

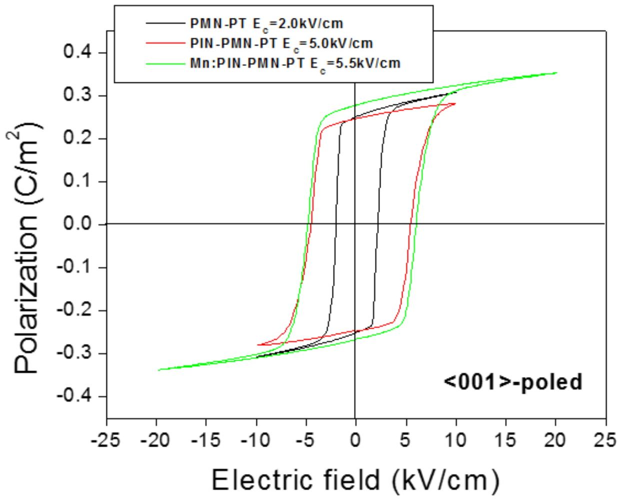

Figure 5. Piezoelectric loop of single crystal composition

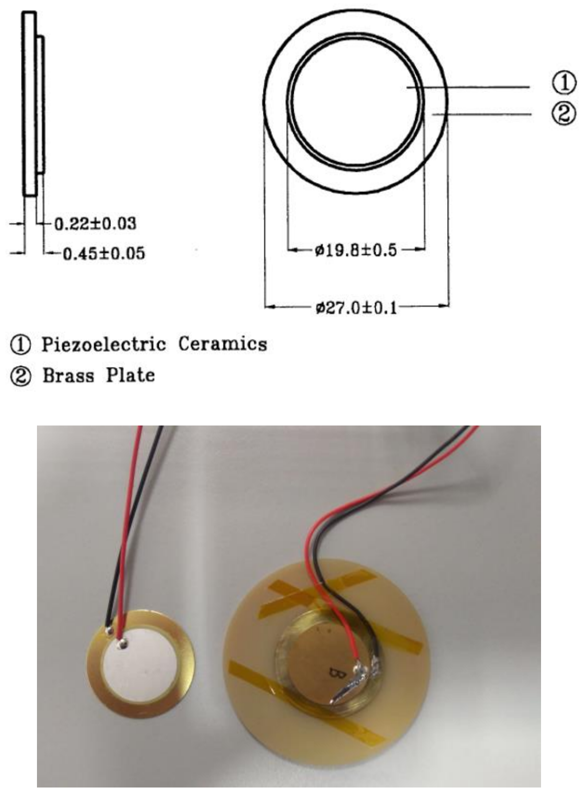

Figure 6. Top: piezoceramic disc geometry; bottom: PZT-5A disc (left) and PMN-PT disc (right, on a protective base)

A summary of the main geometric and physical properties pertaining to the discs and SJA is given in Table 2.

Table 2. Summary of SJA and diaphragm parameters

	Parameter	PZT-5A	PMN-PT
SJA	d (mm)	1.2	
	D (mm)	25	
	h (mm)	2.52 (h/d = 2.1)	
	H (mm)	0.67 (H/d = 0.56)	
Shim	r_D (mm)	13.5	
	t_D (mm)	0.45	
	E (GPa)	103	
	ρ (kg/m^3)	8450	
	υ (-)	0.33	
	k^2 (-)	7.02	
	ξ (-)	0.06	
Piezoceramic	k (-)	0.72	0.93
	E_c (kV/cm)	12	2.0
	tan δ (%)	2.0	0.6
	r_P (mm)	9.9	
	t_P (mm)	0.23	
	E (GPa)	66	115
	ρ (kg/m^3)	7600	8100
	υ (-)	0.31	0.32

A schematic of the SJA is shown in Figure 7. The SJA consists of two parts – a chamber top or orifice plate and a chamber base, which comprises of the cavity when bounded by the orifice plate at the top and the clamped diaphragm at the bottom. The SJA parts were 3D printed out of stainless steel.

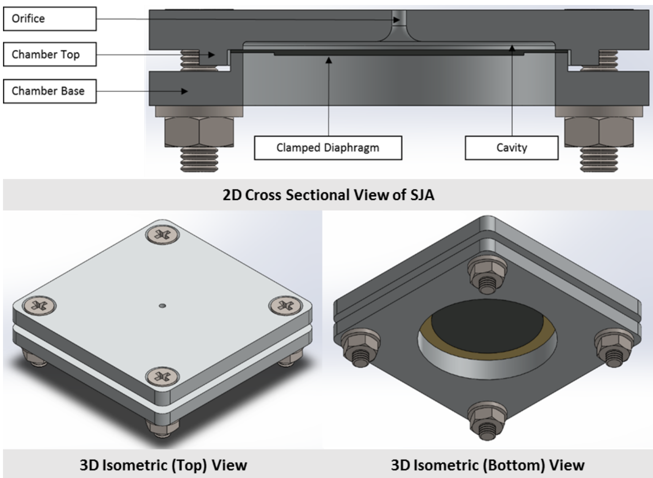

Figure 7. 2D cross section (top) and 3D isometric (bottom) views of the SJA

A SJA device acts like a two-degree of freedom forced mass-spring-damper system with two characteristic resonance frequencies [15-18], which are related to, but not necessarily the same as, the theoretical Helmholtz resonant frequency and mechanical resonant frequency. Helmholtz resonance occurs as a result of a dynamic exchange of kinetic energy of the fluid in the orifice with the potential (pressure) energy of the fluid inside the chamber. The theoretical Helmholtz resonance [19], f_H, is given by Eq. (10)

$$f_H = \frac{a}{2\pi}\sqrt{\left(\frac{d}{D}\right)^2 \frac{1}{H(h+0.85d)}} \tag{10}$$

Where a is the speed of sound. The SJA Helmholtz resonance, f_H=1.69 kHz.

The natural or mechanical resonant frequency of the diaphragm often provides the greatest peak velocity output and thus tends to be more influential than the Helmholtz resonance. It is dependent on the geometric and material properties of the diaphragm. The natural frequency of a circular plate [20], f_D, akin to a SJA diaphragm is given by Eq. (11)

$$f_D = \frac{k^2 t_D}{2\pi r_D^2}\left(\sqrt{\frac{E(1-2\xi)}{12\rho(1-\upsilon^2)}}\right) \tag{11}$$

Where r_D and t_D are the diaphragm radius and thickness, respectively; E, ρ and υ represent the diaphragm material properties (Young's modulus, density and Poisson's ratio, respectively); ξ is the damping coefficient and k^2 is a dimensionless frequency parameter, which is primarily a function of the diaphragm boundary conditions. Table 2 summarises the diaphragm characteristics. The SJA diaphragm resonance, f_D=2.79 kHz.

3.3 Test Procedure

The primary data required to study the power conversion efficiency of the SJA was the input power, diaphragm displacement and jet velocity from the orifice. The test rig, as shown in Figure 8, was built on a 2-axis micro compound table for micrometer scaled position adjustments of the SJA to the hotwire probe and laser vibrometer.

A Trek PZD350A high-voltage piezo amplifier with an output voltage range of 0 to ±350 V DC or peak AC was used to drive the diaphragm. The voltage signal sent to the disc from the amplifier was controlled by a TTI TG215 2 MHz function generator. A fixed sinusoidal voltage waveform was used. Two digital bench multimeters (Model UT801) were connected to the piezo amplifier to provide voltage and current readings. The SJA was tested with two peak voltage inputs, V_{peak} = 10 and 20 V, at excitation frequencies 100 to 4000 Hz in increments of 100 Hz. The voltage input is well within the maximum permissible voltage which, based on E_c = 2.0 kV/cm and t_P = 0.23 mm (Table 2), is V_{peak} = 45 V.

Readings of peak jet velocity were acquired from a Dantec Dynamics 55P11 single hot wire anemometer sensor probe. The sampling frequency was set to 40 kHz and the number of samples was 40,000. For frequency response measurements of the SJA, the probe was positioned centrally at approximately 1*d* from the orifice exit using a vertical micrometer. The percentage error in the velocity measurement using hot-wire anemometry is 3%.

A Microtrak 3 system laser displacement sensor was used to measure the diaphragm peak-to-peak displacement. The laser was offset 50 mm from the centre of the disc. The system uses a sampling frequency of 300 Hz with measurement errors of ± 4 μm, equating to ± 0.4%.

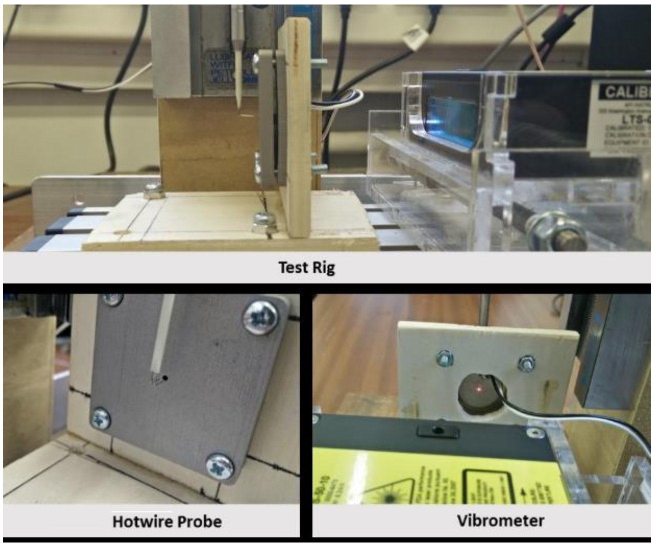

Figure 8. Test setup for hotwire anemometry (jet velocity) and laser vibrometry (diaphragm displacement) measurements

4 Results and Discussion

Figure 9 presents the frequency response of the various SJA characteristics for a fixed diaphragm input voltage of V_{peak}=20 V. For both polycrystalline and single crystal SJAs, a single peak of the peak-to-peak diaphragm displacement, Δ, is observed at f=2.8 kHz (Fig. 9a). This corresponds to the mechanical resonance of the diaphragm and agrees very well with the theoretical value of f_D=2.79 kHz, obtained from Eq. (11). For the PMN-PT SJA, Δ = 87 μm compared with Δ=17 μm for the PZT-5A SJA at f_D and thus the peak diaphragm amplitude of the single crystal device is approximately fivefold that of the polycrystalline device for the same input voltage.

For the peak jet velocity response (Fig. 9b), the maximum velocity of both devices corresponds with f_D. For the PMN-PT SJA, U_{peak}=66 m/s compared with U_{peak}=34 m/s for the PZT-5A SJA, representing a twofold increase of the single crystal device compared with the polycrystalline one. A second velocity peak is visible in the frequency response of the PZT-5A device at f=1.8 kHz. This peak (with U_{peak}=22 m/s) corresponds to the Helmholtz resonance of the SJA cavity and agrees well with the theoretical value of f_H=1.69 kHz, obtained from Eq. (10). By contrast, the velocity peak associated with the Helmholtz resonance is not visible for the PMN-PT device, which has a much more coupled response between f_D and f_H.

Fig. 9c shows the current draw as a function of actuation frequency for both devices. Peak current of both SJAs corresponds with f_D. For the PMN-PT SJA, I_{peak}=55mA compared with I_{peak}=7mA for the PZT-5A SJA, representing an eightfold increase of the single crystal device compared with the polycrystalline one.

(a)

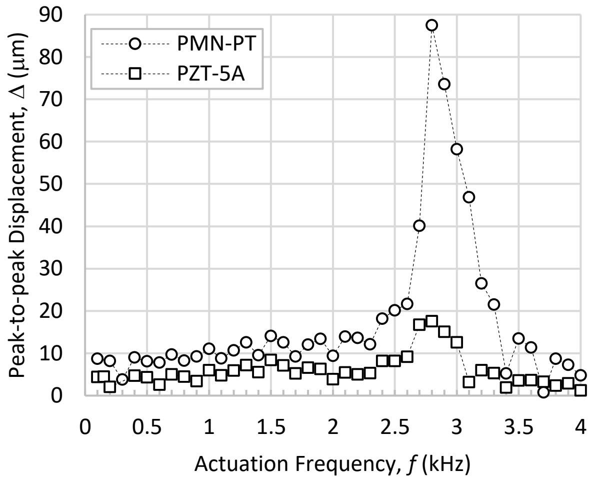

(b)

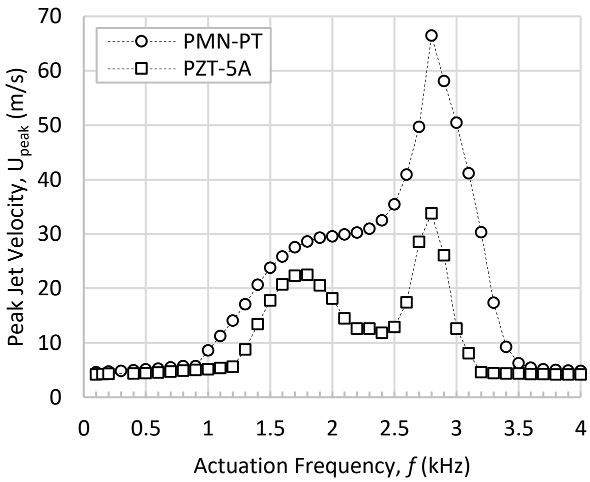

(c)

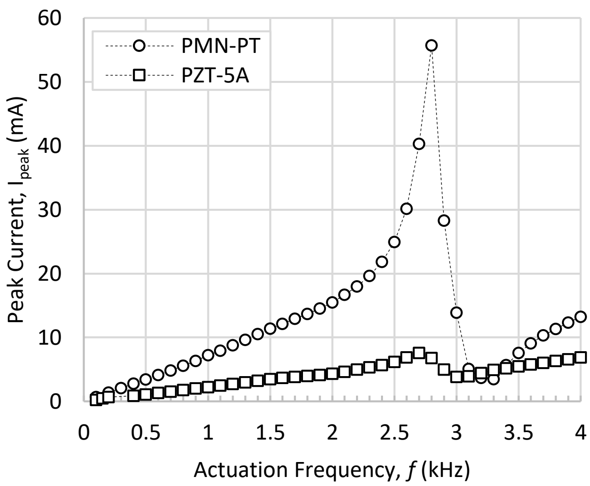

(d)

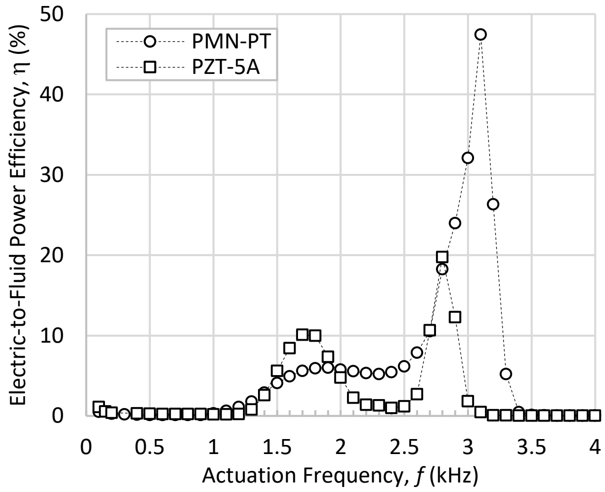

Figure 9. SJA frequency response for V_{peak} = 20 V: (a) peak-to-peak diaphragm displacement, (b) peak jet velocity, (c) peak current and (d) electric-to-fluid power conversion efficiency

Finally, Fig. 9d shows the electric-to-fluidic power conversion efficiency as a function of actuation frequency for both SJA devices. For the PMN-PT SJA, peak efficiency doesn't occur at f_D but at f=3.1 kHz with a value η=47% (at f_D, η=18%). For the PZT-5A SJA, peak efficiency does coincide with f_D with a value η=20%. A second peak, coinciding with f_H, yields an efficiency of η=10%. It's not clear why there is no co-location of peak jet velocity (f=f_D=2.8 kHz) and peak efficiency (f=3.1 kHz) for the PMN-PT SJA. One possible explanation for the non-co-location of conditions between peak jet velocity and peak efficiency is the early onset of dielectric saturation of the piezoceramic patch. A similar mismatch between peak jet velocity and peak efficiency was seen in [2], as shown in Table 1. Despite this, the single crystal device still delivers enhanced performance over the polycrystalline device. For comparable electric-to-fluidic power conversion efficiencies (η ~20%), peak jet velocity of the PMN-PT SJA is twofold larger than the PZT-5A SJA. For comparable peak jet velocities (U_{peak} ~40 m/s), peak efficiency of the PMN-PT SJA is approximately 2.3 times larger than the PZT-5A SJA.

5 Conclusions

This report has documented the first manufacture and test of a single crystal (PMN-PT) piezoceramic synthetic jet actuator (SJA) for more efficient operation. The experimental investigation included laser vibrometry for diaphragm displacement measurements and hotwire anemometry for jet velocity measurements, as well as measurements of electrical power input to the disc. The performance of the single crystal SJA was compared with a SJA using a polycrystalline (PZT-5A) disc of the same geometry. Specific conclusions of the work are as follows:

- For a fixed diaphragm drive voltage (V_{peak}=20 V), the peak-to-peak diaphragm displacement of the PMN-PT SJA is fivefold that of the PZT-5A SJA.
- For comparable electric-to-fluidic power conversion efficiencies (~20%), the peak jet velocity of the PMN-PT SJA is twofold that of the PZT-5A SJA.
- For comparable jet velocities (~40 m/s), the peak electric-to-fluidic power conversion efficiency of the PMN-PT SJA is twofold that of the PZT-5A SJA. At the aircraft systems level, a twofold increase in efficiency would lead to a twofold reduction in overall SJA flow control system mass and power consumption.

References

[1] Mooney, H.P., Brandt, J.B., Lacy, D.S. & Whalen, E.A. 2014. AFC-enabled vertical tail integration study, NASA/CR-2014-218168.

[2] Crowther, W.J. & Gomes, L.T., 2008. An evaluation of the mass and power scaling of synthetic jet actuator flow control technology for civil transport aircraft applications. *Proc. IMechE. Part I: Journal of Systems and Control Engineering*, 222, pp. 357-372.

[3] Slipher, G.A. & Hubbard Jr, J.E., 2007. Description and characterisation of an electroactive polymer synthetic jet actuator. *Proc. SPIE – Electroactive Polymer Actuators and Devices*, 6524, pp. 1-12.

[4] Liang, Y., Kuga, Y. & Taya, M., 2005. Design of synthetic jet actuator based on FSMA composite. *Proc. SPIE – Smart Structures and Materials*, 5762, pp. 179-186.

[5] Santhanakrishnan, A. & Jacob, J.D., 2007. Flow control with plasma synthetic jet actuators. *Journal of Physics D: Applied Physics*, 40, pp. 637-651.

[6] Disc Benders: Piezo Unimorph and Bimorphs, APC International Ltd., Accessed: 1 July 2018. https://www.americanpiezo.com/standard-products/disc-benders.html

[7] Buren, T.V., Whalen, E. & Amitay, M., 2015. Achieving a high-speed and momentum synthetic jet actuator. *Journal of Aerospace Engineering*, 29, pp. 04015040-1 – 04015040-16.

[8] Feero, M.A., Lavoie, P. & Sullivan, P.E., 2015. Influence of activity shape on synthetic jet performance. *Sensors and Actuators A: Physical*, 223, pp. 1-10.

[9] Jabbal, M. & Jeyalingam, J., 2017. Towards the noise reduction of piezoelectrical-driven synthetic jet actuators. *Sensors & Actuators A: Physical*, 266, pp. 273-284.

[10] Li, R., Sharma, R. & Arik, M., 2011. Energy conversion efficiency of synthetic jets. *Proc.*

ASME 2011 Pacific Rim Technical Conference and Exhibition on Packaging and Integration of Electronics and Photonic Systems, MEMS and NEMS, InterPACK 2011, Portland, Oregon, USA, 6-8 July, 2011.

[11] Girfoglio, M., Greco, C.S., Chiatto, M. & de Luca, L., 2015. Modelling of efficiency of synthetic jet actuators. *Sensors & Actuators A: Physical*, 233, pp. 512-521.

[12] Seele, R., Graff, E., Lin, J. & Wygnanski, I., 2013. Performance enhancement of a vertical tail model with sweeping jet actuators. *Proc. 51st AIAA Aerospace Sciences Meeting*, AIAA 2013-0411, Grapevine, Texas, USA, 7-10 January, 2013.

[13] Rusovici, R. & Lesieutre, G.A., 2004. Design of a single-crystal piezoceramic-driven synthetic jet actuator, *Proc. SPIE 5390, Smart Structures and Materials 2004: Smart Structures and Integrated Systems*, doi: 10.1117/12.539576.

[14] Jabbal, M., 2009. Flow control actuators for the 2020 civil transport aircraft. EU FP6 AVERT Report, AST5-CT-2006-030914.

[15] Gallas, Q., Holman, R., Nishida, T., Carroll, B., Sheplak, M. & Cattafesta, L., 2003. Lumped element modelling of piezoelectrical-driven synthetic jet actuators. *AIAA Journal*, 41, pp. 240-247.

[16] Sharma, R.N., 2007. Fluid-dynamics-based analytical model for synthetic jet actuation. *AIAA Journal*, 45, pp. 1841-1847.

[17] Persoons, T., 2012. General reduced-order model to design and operate synthetic jet actuators. *AIAA Journal*, 50, pp. 916-927.

[18] de Luca, L., Girfoglio, M. & Coppola, G., 2014. Modelling and experimental validation of the frequency response of synthetic jet actuators. *AIAA Journal*, 52, pp. 1733-1748.

[19] Tang, H. & Zhong, S., 2007. A static compressible flow model of synthetic jet actuators. *The Aeronautical Journal*, 111, pp. 421-431.

[20] Jabbal, M., Liddle, S., Potts, J. & Crowther, W., 2013. Development of design methodology for a synthetic jet actuator array for flow separation control applications. *Proc. IMechE. Part G: Journal of Aerospace Engineering*, 227, pp. 110-124.